Int j simul model 24 (2025) 2, 333-344
Original scientific paper

MICRO-TEXTURE OPTIMIZATION FOR TITANIUM CUTTING TOOLS VIA SIMULATION

Wu, D.; Zhao, C. L.[#]; Huang, C. L. & Luo, X.
School of Intelligent Manufacturing, Geely University of China, Chengdu 641423, China
E-Mail: zhaochenlei2025@163.com

Abstract
This study presents optimization of micro-texture parameters for titanium alloy cutting tools to enhance machining performance. A two-dimensional finite element model was developed in the ABAQUS environment, incorporating the Johnson-Cook constitutive model to simulate the cutting process of Ti6Al4V (TC4) titanium alloy. The effects of micro-texture width, spacing, depth, and distance from the tool edge on cutting force and temperature were systematically investigated using an orthogonal experimental design. Simulation results demonstrated that micro-textured tools significantly reduced cutting forces and temperatures compared to non-textured tools, with optimal parameter combinations achieving reductions of up to 72.6 % in cutting force and 189°C in temperature. Range analysis revealed the hierarchical influence of micro-texture parameters: distance from the edge had the greatest impact on cutting force, while texture width most strongly affected temperature. The study reveals critical mechanical-thermal trade-offs in micro-textured tool design, necessitating multi-objective optimization to guide high-performance titanium machining applications.
(Received in January 2025, accepted in May 2025. This paper was with the authors 6 weeks for 2 revisions.)

Key Words: Micro Texture Tool, Parameter Optimization, Cutting Force, Cutting Temperature

1. INTRODUCTION

Titanium alloys, known for their high strength-to-weight ratio, corrosion resistance, and biocompatibility, are critical in aerospace, medical, and automotive industries. However, their machinability is challenging due to high hardness, low thermal conductivity, and work hardening tendencies. These factors cause rapid tool wear, increased cutting forces, and poor surface finish, necessitating advanced cutting tools and methodologies. Micro-texturing, a surface engineering technique, enhances cutting tool performance by altering lubricant flow, reducing friction and wear, and improving heat dissipation. Studies have optimized micro-texture parameters to maximize tool life, minimize cutting forces, and improve surface quality [1]. For example: Liu et al. [2] used surrogate-based optimization methods (e.g., Kriging models) to identify texture parameters that significantly reduce friction coefficients. Qi et al. [3] designed orthogonal experiments considering edge distance, texture width, and spacing, determining optimal parameters through range analysis. Li et al. [4] found that optimized micro-textured tools outperformed non-textured ones in cutting force, temperature, and chip-breaking ability. Despite progress, existing research focuses on specific materials or applications, with limited attention to titanium alloy cutting tools. Optimization often relies on trial-and-error or traditional experimental designs, which are time-consuming and resource-intensive. Additionally, the interaction between micro-texture geometry, cutting conditions, and material properties remains poorly understood, hindering the development of generalized predictive models.

This study proposes a simulation-based optimization framework for micro-texture parameters of titanium alloy cutting tools. It addresses the limited understanding of how micro-textures influence cutting performance and the inefficiencies of existing optimization methods [5, 6]. By employing advanced simulation techniques, the study investigates the interaction mechanisms between micro-textures and titanium alloys during the cutting process. The key contributions are as follows: ① Development of a finite element model that simulates material deformation, heat generation, and tool-chip interactions, enabling accurate predictions of cutting forces, temperatures, and wear. ② Optimization of micro-texture parameters (shape, size, orientation, and distribution) using response surface methodology (RSM) and advanced algorithms to maximize tool life, minimize cutting forces, and improve surface finish [7]. ③ Detailed analysis of how micro-textures enhance cutting performance through lubricant flow, chip formation, and tool-chip contact conditions [8]. ④ Establishment of generalized models and guidelines for designing micro-textured tools, providing valuable references for both manufacturers and researchers. Using ABAQUS software, we simulated the behaviour of micro-textured tools during titanium alloy machining, generating comprehensive datasets for cutting forces and temperatures. Orthogonal experimental results were analysed using range analysis, followed by univariate analysis to identify optimal parameter combinations [9]. This framework significantly enhances the development of high-performance cutting tools, thereby improving machining efficiency and quality in critical industries.

2. RESEARCH MODEL

2.1 Geometric model and grid generation

In the external cylindrical turning process, the cutting tool can be conceptually regarded as moving relative to a stationary workpiece at the specified cutting speed along the surface of the workpiece. To simplify the analysis and improve computational accuracy, the three-dimensional finite element stress problem was converted to a two-dimensional plane strain formulation. The workpiece and tool were projected onto the base plane to define the simulation domain. The micro-textured cutting tool's two-dimensional geometric model was created in ABAQUS using YG6 cemented carbide as the tool material, as shown in Fig. 1.

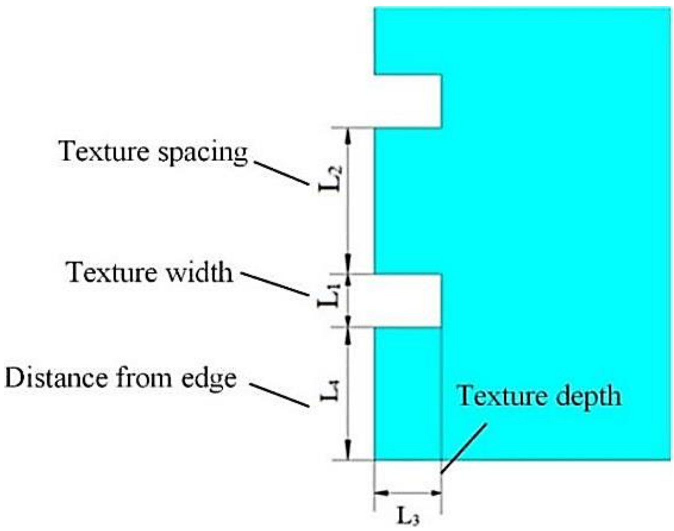

Figure 1: Geometric model of micro-textured tool.

The finite element model meshing is illustrated in Fig. 2 The workpiece material is titanium alloy TC4, with geometric dimensions of 2.00 mm × 1.00 mm. The titanium alloy workpiece was discretized using eight-node thermo-structural coupled quadrilateral elements, and a reduced integration method was employed for structured meshing [10]. To optimize computational efficiency while maintaining accuracy, a refined mesh with an element size of 0.01 mm × 0.01 mm was applied to the machined surface of the workpiece to achieve precise results [11]. In contrast, the non-machined regions of the workpiece and the cutting tool were meshed with quadrilateral elements sized at 0.5 mm × 0.5 mm.

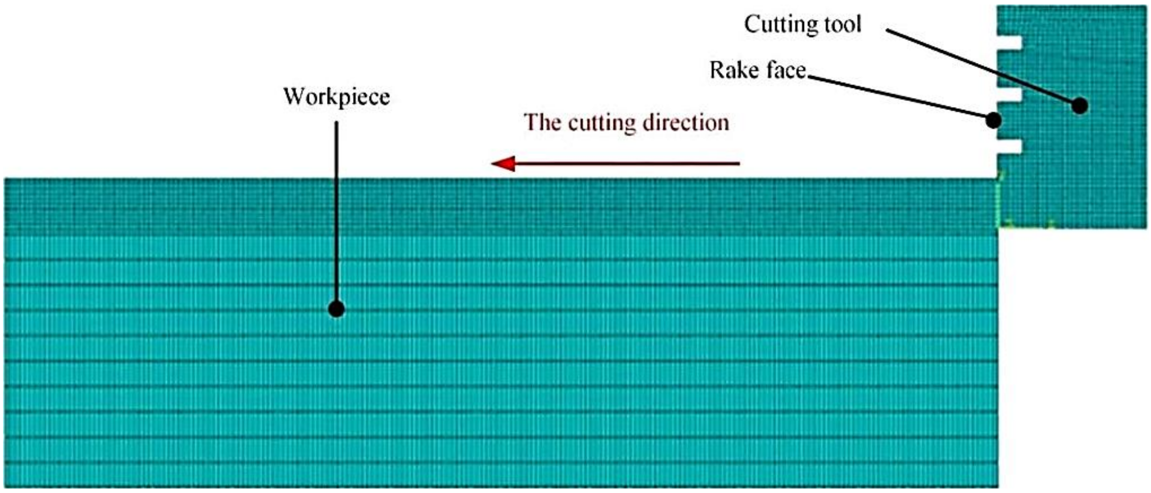

Figure 2: Mesh of finite element model.

2.2 Material characteristics and cutting conditions

In the ABAQUS pre-processing interface, the workpiece dimensions are set to 2 mm in length and 1 mm in height, with Ti6Al4V (TC4) as the material and WC as the tool material. Material parameters for both the tool and workpiece are listed in Table I. The simulation time is set to 0.005 s, with a cutting depth of 0.1 mm and a cutting speed of 240 m/min. General contact is used in the interaction module, and the cutting tool has a rake angle and clearance angle of 0°, with a sharp edge (cutting edge radius = 0 mm) [12]. Finite element settings align with those reported by Wu et al. [13]. Plane stress conditions are applied to the free side to accurately reflect buckling or deformation caused by cutting forces. The heat exchange coefficient between the workpiece, tool, and air is 0.02 N/(s·mm·K), while the coefficient between the tool and workpiece is 45 N/(s·mm·K).

Table I: Tool and workpiece material parameters.

Property	Cutter	Workpiece
Density (kg/m^3)	14850	4450
Young's modulus	640	112
Poisson's ratio	0.22	0.34
Coefficient of thermal expansion (10^{-6}/°C)	4.7	9.3
Thermal conductivity (W/(m/°C)	76.9	6.8
Specific heat (J/(kg/°C))	176	565

2.3 Material constitutive model setting

In the cutting simulation, the choice of the material constitutive model is very important to the simulation accuracy. The commonly used material models include the Johnson-Cook model, the Power Law model, and the Steinberg model. For titanium alloy material, considering the effects of the temperature, deformation, and strain rate on the cutting process, Johnson-Cook's empirical model, which is widely used in the world, is selected as the constitutive model, which is given by Eq.(1) [14].

$$\overline{\sigma} = (A + B\varepsilon^n) \cdot \left[1 + CIn\frac{\dot{\varepsilon}}{\varepsilon_0}\right] \cdot \left[1 - \left(\frac{T - T_r}{T_m - T_r}\right)^m\right] \tag{1}$$

where $\overline{\sigma}$ is the flow stress, A, B, n, C and m are the material's inherent parameters, T_m is the melting point of the material, T_r is the reference temperature, ε_0 is the reference plastic strain rate, ε^n is the equivalent plastic strain, and $\dot{\varepsilon}$ is the plastic strain rate. The inherent parameters of the material can be obtained through experiments. In this study, the inherent parameters *A*, *B*, *n*, *C* and *m* for the TC4 alloy used in the Johnson-Cook model are 968.88 MPa, 567.17 MPa, 0.0394, 0.375 and 1, respectively [15].

3. SIMULATION EXPERIMENT AND RESULTS

3.1 Settings of the simulation experiment

Based on the predetermined cutting parameters, this study quantitatively investigated the effects of micro-texture parameters – texture width (L_1), texture spacing (L_2), texture depth (L_3), and distance from the cutting edge (L_4) – on cutting force and cutting temperature. An $L_9(3^4)$ orthogonal array experimental design was employed, incorporating four factors at three levels (Level 1, Level 2, and Level 3), as detailed in Table II. Test number T-00 is the control group (no micro-texture) [16]. The cutting force simulation experiment is carried out with nine groups of data using ABAQUS software. In each set of simulations, the preset simulation steps are strictly followed to ensure that the other influencing factors are consistent, except for the four key variables of the texture width, texture spacing, texture depth, and distance from the edge. At the end of each simulation, the data for the stable stage within 0.00015–0.00045 s of the time history are selected for processing [17].

Table II: Cutting simulation experimental factor level table.

Factor Levels	**Texture width (A)**	**Texture spacing (B)**	**Texture depth (C)**	**Distance from the edge (D)**
Level 1	20	75	25	50
Level 2	30	100	50	100
Level 3	40	125	75	150

3.2 Experimental result

(1) Experimental results of cutting force and cutting temperature

The cutting force curve data are output in the direction of the main cutting force *F* at the post-processing interface, the average value for the main cutting force is calculated while recording the highest tool temperature at this stage, and the orthogonal table is filled in. The final experimental data results are shown in Table III.

Table III: Orthogonal experiment results.

Serial number factor	**A**	**B**	**C**	**D**	**Average value of main cutting force *F* (N)**	**Maximum cutting temperature *T* (°C)**
	L_1/μm	L_2/μm	L_3/μm	L_4/μm		
T-00	0	0	0	0	431	909
T-01	20	75	25	50	134	720
T-02	20	100	50	100	123	797
T-03	20	125	75	150	122	817
T-04	30	75	50	150	123	841
T-05	30	100	75	50	123	865
T-06	30	125	25	100	119	828
T-07	40	75	75	100	118	821
T-08	40	100	25	150	120	837
T-09	40	125	50	50	148	868

(2) Experimental result verification

The author verified the accuracy of the finite element method employed in this paper by utilizing the finite element setup from the literature by Wu et al. [13]. A cutting simulation analysis was performed using the dynamic display module in the commercial software ABAQUS CAE, where the Conventional Tool model from the literature was established. The material parameters and finite element settings were consistent with those reported in the literature.

Cutting temperatures and cutting forces at various cutting speeds were extracted, and the results were compared with those in the literature, as illustrated in Fig. 3. Fig. 3 a depicts the relationship between cutting temperature and cutting speed; it is evident that as the cutting speed increases, the cutting temperature also rises, with the results obtained closely matching the experimental findings in the literature. Furthermore, as shown in Fig. 3 b, the relationship between chip temperature and cutting speed was also analysed. As the cutting speed increases, the cutting force tends to decrease, which is consistent with the experimental results. Therefore, it can be concluded that the finite element setup established in this paper is valid and suitable for subsequent analyses.

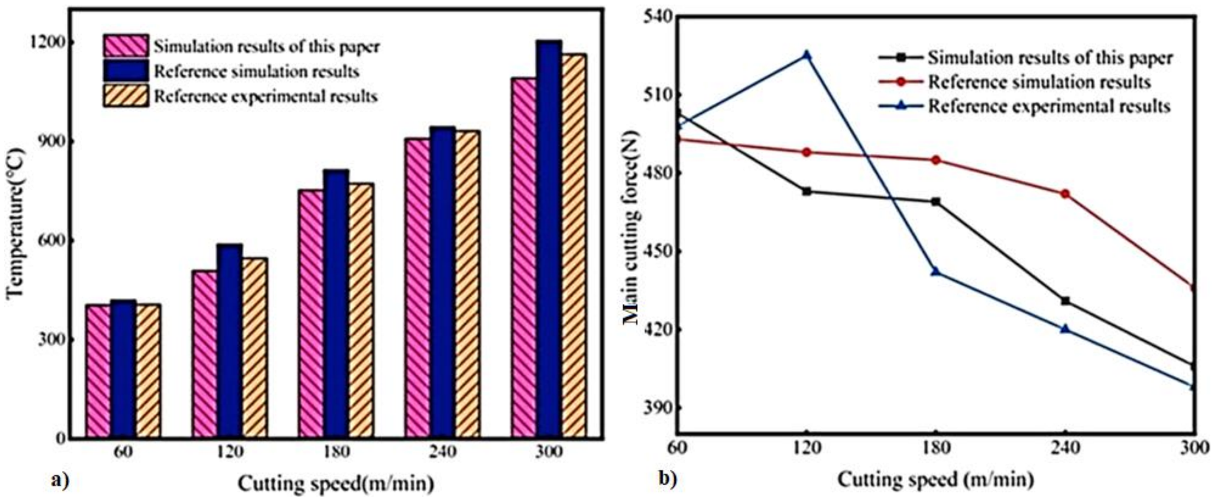

Figure 3: Comparison of simulation results with experimental results from the literature: a) Cutting temperature vs. cutting speed; b) Cutting force vs. cutting speed.

3.3 Discussion of the results

(1) Effect of combined micro-texture parameters on cutting force

Cutting force is a key indicator of tool performance. As shown in Table III, textured tools consistently generate lower principal cutting forces than non-textured tools throughout the process, with reductions varying by degree. This is mainly due to the reduced contact area between the chip and the tool caused by micro-textures, which lowers frictional force at the interface and reduces cutting resistance. A comparison of textured tools reveals that micro-texture geometry significantly affects cutting force. For example, tool T-07 achieves the lowest principal cutting force of 118 N, a 72.6 % reduction from the non-textured tool's 431 N. While tool T-09 has the highest cutting force (148 N) among textured tools, it still reduces cutting force by 65.7 % compared to the non-textured tool [18, 19].

A comparative analysis of the principal cutting force for tools T-00 and T-07 (Fig. 4) shows similar trends: an initial rapid increase, followed by stabilization and fluctuations within a specific range. However, T-07 exhibits more frequent fluctuations than T-00. During cutting, compression of the workpiece causes a sharp rise in cutting force. Material separation and chip curling then lead to fluctuations in cutting force. For T-00, chips slide frictionally along the rake face after passing the cutting edge. In contrast, micro-textures on T-07 cause frequent contact between the chip and texture edges during sliding, increasing contact frequency and resulting in higher fluctuation frequency compared to T-00.

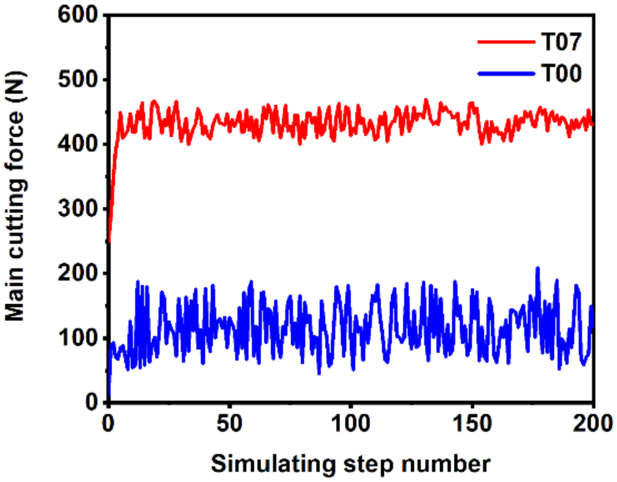

Figure 4: Comparison of main cutting forces.

(2) Effect of combined micro-texture parameters on cutting temperature

As evidenced by the data presented in Table III, the maximum temperatures recorded for micro-textured tools during cutting operations are consistently lower than those for non-textured tools. This thermal advantage can be attributed to the surface micro-textures, which serve dual functions: ① reducing frictional forces at the tool-chip interface, thereby minimizing frictional heat generation, and ② enhancing air circulation at the interface, which facilitates improved heat dissipation. Furthermore, the micro-textured tools promote enhanced chip curling during cutting, effectively reducing the tool-chip contact area and consequently decreasing both heat generation and thermal transfer. Among the various micro-textured tools with different geometric parameters, the temperature reduction effects vary significantly. Tool T-01 demonstrates the most substantial temperature reduction, with a maximum temperature of 720°C, representing a decrease of 189°C compared to the non-textured tool. In contrast, tool T-09 shows a relatively moderate reduction, reaching a maximum temperature of 868°C, which is 41°C lower than that of its non-textured counterpart [20]. Fig. 5 illustrates the temperature distribution during the cutting process at the 100th step of steady-state cutting.

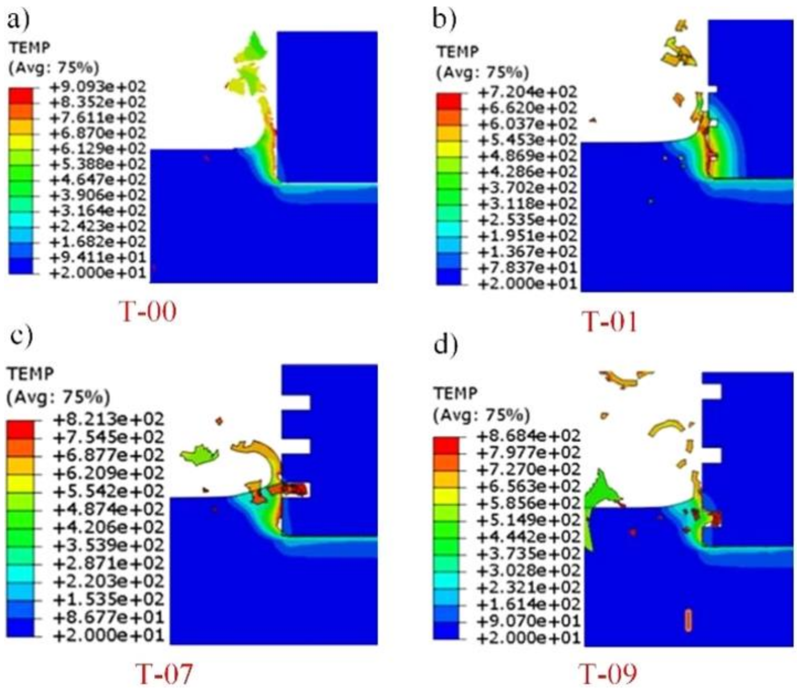

Figure 5: Temperature distribution during cutting.

As illustrated in Fig. 5, the maximum cutting temperatures are predominantly concentrated in the contact zone between the workpiece and the cutting tool. The conventional tool (T-00) exhibits a broad temperature distribution with relatively low chip curl, while the micro-textured tools (T-01, T-07, T-09) demonstrate enhanced chip curl and generate significant chip fragmentation. Among these, T-07 exhibits the most pronounced chip curl, whereas T-09 produces the most substantial chip fragmentation. The increased chip curl effectively reduces the tool-chip contact area, thereby limiting heat generation and thermal transfer. The temperature distribution of the micro-textured tools is more concentrated, with reduced high-temperature zones and expanded low-temperature regions, particularly evident in T-01. This phenomenon can be primarily attributed to the secondary cutting effect of the groove edges, which facilitates efficient chip evacuation. In contrast, T-09 demonstrates less effective secondary cutting at the micro-groove edges, resulting in substantial chip accumulation within the micro-grooves and impaired chip evacuation [19]. Consequently, this diminishes the tool's effectiveness in reducing cutting forces and improving heat dissipation. Furthermore, the significant chip fragmentation observed in the micro-textured tools can be ascribed to the disruption of thermal continuity by the micro-textures, which expands the heat dissipation area. This inhibits heat conduction into the tool interior and promotes rapid heat evacuation through chip removal. These findings provide compelling evidence that an optimized combination of micro-texture parameters can effectively reduce the tool-chip contact area, subsequently lowering both cutting forces and temperatures during machining operations [21].

(3) Discussion on the Influence of Factor Level Variations on Experimental Results

Range analysis involves aggregating experimental results for a specific factor at the same level, as shown in Table II, which summarizes the total cutting forces or temperatures for three groups corresponding to different factor levels. Averages are then calculated for each level. The range (*R*), defined as the difference between the maximum and minimum averages, indicates the significance of a factor's influence. A larger range signifies a stronger impact on the experimental outcomes [22]. Applying range analysis to the data in Table III yielded the results summarized in Tables IV and V.

Tables IV: Range analysis of main cutting force (*F*).

Range parameter	L_1/μm	L_2/μm	L_3/μm	L_4/μm
K_1	379	375	373	405
K_2	365	366	394	360
K_3	386	389	363	365
$\overline{K_1}$	126	125	124	135
$\overline{K_2}$	121	122	131	120
$\overline{K_3}$	128	130	121	122
R	7	8	10	15
Optimal level	2	2	3	2

The influence hierarchy of micro-texture parameters on the main cutting force (*F*) is as follows (in descending order): $L_4 > L_3 > L_2 > L_1$. Optimization analysis aimed at minimizing the main cutting force identified the optimal levels as: L_1 = 30 μm, L_2 = 100 μm, L_3 = 75 μm, L_4 = 100 μm. For cutting temperature (*T*), the influence ranking differs: $L_1 > L_2 > L_3 > L_4$. The optimal levels for minimizing temperature were found to be: L_1 = 20 μm, L_2 = 75 μm, L_3 = 25 μm, L_4 = 100 μm. To intuitively illustrate the effects of micro-texture parameters on cutting force and temperature, line graphs are plotted in Fig. 6.

Tables V: Range analysis of cutting temperature (*T*).

Range parameter	L_1/μm	L_2/μm	L_3/μm	L_4/μm
K_1	2334	2382	2385	2453
K_2	2534	2499	2506	2446
K_3	2526	2513	2503	2495
$\overline{K_1}$	778	794	795	818
$\overline{K_2}$	845	833	835	815
$\overline{K_3}$	842	838	834	832
R	67	44	40	17
Optimal level	1	1	1	2

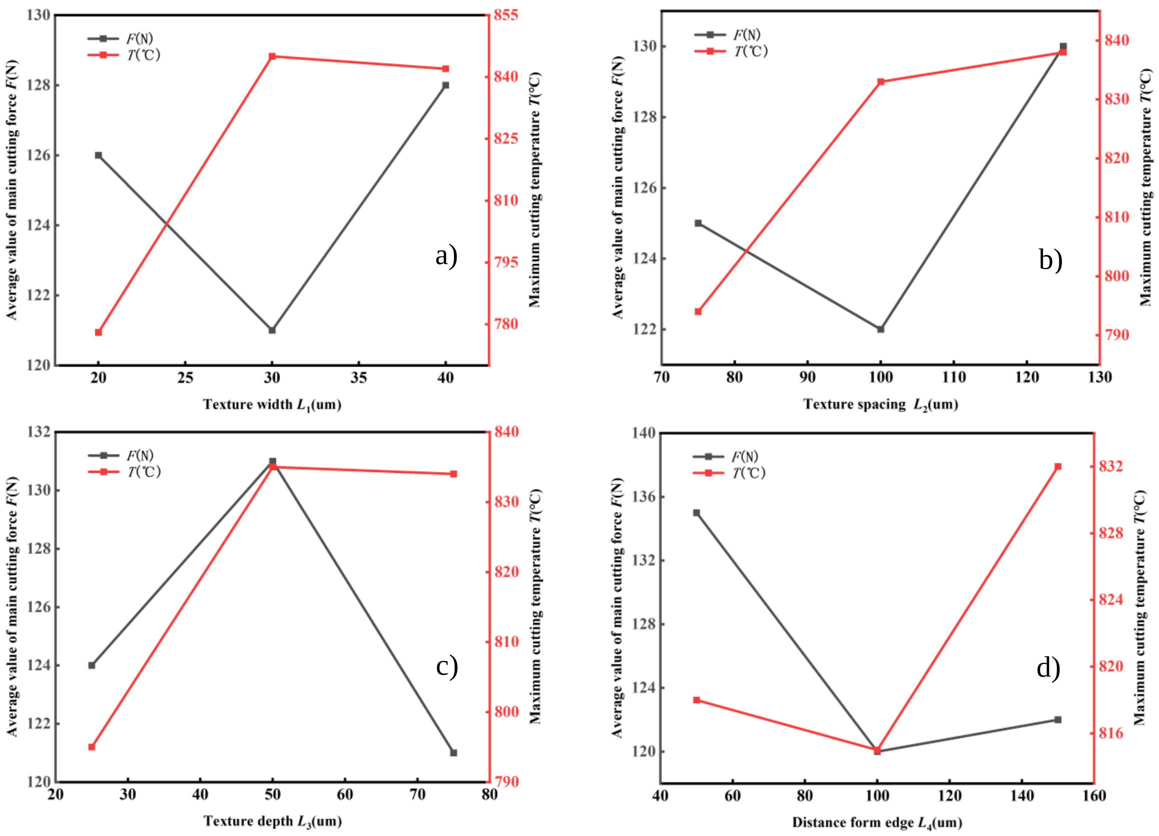

Figure 6: The influence of texture parameters on physical parameters: a) The influence of texture width on physical parameters; b) The influence of texture spacing on physical parameters; c) The influence of texture depth on physical parameters; d) The influence of the distance from the edge on physical parameters.

As shown in Fig. 6 a, the average cutting force decreases significantly with increasing micro-texture width within a specific range, but slows or reverses beyond a critical threshold. This indicates an optimal width for minimizing cutting forces, as excessive width may degrade performance. Conversely, cutting temperature initially increases with wider textures, then stabilizes or decreases beyond a certain point, confirming an optimal range for thermal control. The opposing effects of micro-texture width on cutting force and temperature present a trade-off: wider textures reduce mechanical loads but increase thermal loads. Practical implementation requires optimizing micro-texture width based on operational constraints and priorities to balance force reduction and temperature management [23].

As shown in Fig. 6 b, the average cutting force decreases significantly with increasing micro-texture spacing up to a critical threshold, after which the reduction slows or reverses. This indicates that optimal spacing enhances machining efficiency by reducing cutting forces. In contrast, cutting temperature increases with spacing but stabilizes or declines after reaching a peak beyond an optimal range. The opposing effects of micro-texture spacing on cutting force and temperature present a trade-off in machining optimization [24]. Practical applications require balancing these parameters to achieve optimal performance. The non-monotonic relationships emphasize the importance of identifying critical spacing thresholds for process optimization.

As illustrated in Fig. 6 c, the average cutting force exhibits an initial variation trend with increasing micro-texture depth. Based on the observed pattern, we hypothesize that the cutting force demonstrates a decreasing tendency with greater texture depth, suggesting that deeper micro-textures may facilitate reduced mechanical loads during machining. However, this relationship appears to be non-linear, as the force reduction effect tends to saturate beyond a critical depth threshold, potentially even reversing its trend. In contrast, the cutting temperature manifests an opposing behaviour profile. The experimental data suggest a probable positive correlation between texture depth and temperature elevation, indicating that deeper micro-textures might intensify thermal generation during cutting operations. Similarly, this thermal response follows a non-linear pattern, reaching an inflection point beyond which the temperature either stabilizes or begins to decline [25]. The complex and often contradictory influences of micro-texture depth on both mechanical and thermal aspects of machining present a significant optimization challenge. These findings emphasize the necessity for a comprehensive, multi-objective optimization approach when determining the optimal micro-texture depth in practical applications, particularly when balancing between force reduction and temperature control requirements.

From Fig. 6 d, it can be observed that the average cutting force exhibits a nonlinear trend of initially decreasing and then increasing with the increase in distance from the edge. This variation may indicate that there is a specific range of distances from the edge within which the cutting force reaches a minimum value, thereby optimizing the cutting performance. Based on the trend shown in the figure, it can be hypothesized that the average cutting force decreases with an increase in micro-texture depth, suggesting that increasing micro-texture depth contributes to reducing the average cutting force during the cutting process. However, this trend may not be linear, and the change in average cutting force may plateau or even reverse when the micro-texture depth reaches a certain level [26]. In contrast to the variation in average cutting force, the cutting temperature may exhibit an opposite trend with the increase in micro-texture depth. Assuming an opposite change based on the figure's trend, the cutting temperature may rise as the micro-texture depth increases, indicating that increasing micro-texture depth may lead to an elevation in cutting temperature. Similarly, this trend may also be nonlinear, and the change in cutting temperature may level off or start to decline when the micro-texture depth reaches a specific value. The influence of micro-texture depth on average cutting force and cutting temperature is complex and may involve conflicting effects. Therefore, it is necessary to comprehensively consider both influences in practical applications to identify the optimal micro-texture depth [27].

3.4 A trade-off between cutting force and temperature reduction

In industrial machining processes, minimizing cutting forces and reducing cutting temperatures are critical objectives for enhancing tool performance. The range analysis of these dual performance metrics reveals that their individual optimal parameter combinations are not identical, necessitating a balanced optimization approach based on the relative influence of each factor. The analytical results demonstrate that: ① Texture width (L_1) should be optimized primarily for cutting force reduction, selecting Level 2 (20 μm). ② Texture spacing (L_2) and depth (L_3) should prioritize temperature control, adopting Level 1 (75 μm and 25 μm respectively). ③ Edge distance (L_4) at Level 2 (100 μm) exhibits the most favourable compromise, simultaneously minimizing both cutting force and temperature compared to baseline values. Thus, the comprehensive optimal parameter combination is determined as: $L_1 = 20$ μm, $L_2 = 75$ μm, $L_3 = 25$ μm, $L_4 = 100$ μm.

4. CONCLUSION

This study systematically investigated the effects of micro-texture parameters on the cutting performance of titanium alloy (Ti6Al4V) tools through finite element simulation and orthogonal experimental design. The key findings and conclusions are summarized as follows:

(1) Performance enhancement: Micro-textured tools consistently outperformed non-textured tools, demonstrating significant reductions in cutting force (up to 72.6 %) and cutting temperature (up to 189°C). The optimized micro-texture parameters effectively reduced tool-chip contact area, friction, and heat generation, thereby improving machining efficiency.

(2) Parameter analysis and optimization: Range analysis revealed that the distance from the cutting edge (L_4) had the strongest influence on cutting force, while micro-texture width (L_1) most significantly affected cutting temperature. Optimal micro-texture parameter combination determined through comprehensive consideration of cutting force and temperature: $L_1 = 20$ μm, $L_2 = 75$ μm, $L_3 = 25$ μm, $L_4 = 100$ μm.

(3) Mechanistic performance trade-offs: A distinct trade-off exists between cutting force reduction and temperature control, where increased micro-texture width lowers cutting force but raises temperature, necessitating multi-objective optimization. Mechanistically, micro-textures enhance chip curling and fragmentation, reducing tool-chip contact area and improving heat dissipation. However, excessive texture dimensions (e.g., depth/spacing) may compromise chip evacuation, thereby increasing thermal loads and offsetting performance benefits.

(4) Validation and applicability: The simulation methodology was validated against experimental literature data, confirming its reliability for optimizing micro-texture designs. The findings provide actionable guidelines for designing high-performance cutting tools for titanium alloy machining, with potential applications in aerospace and biomedical industries.

(5) Limitations of the current study: the 2D simulation model simplifies complex 3D cutting phenomena, and the study assumes ideal conditions without considering tool wear effects. Additionally, the findings are specific to Ti6Al4V under the tested cutting parameters.

ACKNOWLEDGEMENT

This work has been funded by the Planning Project of the Science and Technology Department of Sichuan Province, China (Grant Number: 20QYCX0073). We are profoundly grateful to Professor Zhang Wenchao for his invaluable guidance and suggestions on research design and data analysis. His profound insights have significantly enhanced our comprehension of the research problems and have refined our research methodologies.

REFERENCES

[1] Păun, M.-A.; Coandă, H.-G.; Mincă, E.; Iliescu, S. S.; Duca, O. G.; Stamatescu, G. (2024). Improved multi-objective genetic algorithm used to optimizing power consumption of an integrated system for flexible manufacturing, *Studies in Informatics and Control*, Vol. 33, No. 1, 27-36, doi:10.24846/v33i1y202403

[2] Liu, S.; Li, B.; Gan, R.; Xu, Y.; Yang, G. (2023). Surrogate-based optimization design for surface texture of helical pair in helical hydraulic rotary actuator, *Scientific Reports*, Vol. 13, Paper 20259, 19 pages, doi:10.1038/s41598-023-47509-7
[3] Qi, Z.-X.; Chen, X.-M.; Liu, Y.; Wang, L. (2023). Optimization of texture parameters of combined micro-texture tools, *Equipment Machinery*, Vol. 2023, No. 1, 32-36, doi:10.3969/j.issn.1662-0555.2023.01.007
[4] Li, B.-B.; Chen, L.; Zhao, W.; Yu, M.; Zhang, K. (2020). Simulation study on optimization of texture parameters of micro-texture tools, *Modern Manufacturing Engineering*, Vol. 2020, No. 10, 91-96, doi:10.16731/j.cnki.1671-3133.2020.10.016
[5] Damjanović, S.; Katanić, P.; Zavadskas, E. K.; Stević, Ž.; Krsmanović, B.; Djalić, N. (2024). Novel fuzzy MCDM model for comparison of programming languages, *Studies in Informatics and Control*, Vol. 33, No. 4, 5-14, doi:10.24846/v33i4y202401
[6] Haddouche, R.; Chetate, B.; Boumedine, M. S. (2019). Neural network ARX model for gas conditioning tower, *International Journal of Modelling and Simulation*, Vol. 39, No. 3, 166-177, doi:10.1080/02286203.2018.1538848
[7] Angelakis, C.; Loukis, E. N.; Pouliezos, A. D.; Stavrakakis, G. S. (2001). A neural network-based method for gas turbine blading fault diagnosis, *International Journal of Modelling and Simulation*, Vol. 21, No. 1, 51-60, doi:10.1080/02286203.2001.11442186
[8] Boudelier, A.; Ritou, M.; Garnier, S.; Furet, B. (2011). Optimization of process parameters in CFRP machining with diamond abrasive cutters, *Advanced Materials Research*, Vol. 223, 774-783, doi:10.4028/www.scientific.net/AMR.223.774
[9] Agari, S. R.; Lakshmikanthan, A.; Selvan, C. P.; Vijay Sekar, K. S. (2024). Improvement in the machining processes by micro-textured tools during the turning process, *Engineering Proceedings*, Vol. 61, No. 1, Paper 2, 9 pages, doi:10.3390/engproc2024061002
[10] Han, P.; Yang, S.;·Tong, X. (2023). Study on surface integrity enhancement of titanium alloy milling with ball end mill by micro-texture, *The International Journal of Advanced Manufacturing Technology*, Vol. 125, Nos. 11-12, 5697-5712, doi:10.1007/s00170-023-10901-8
[11] Gang, L. (2024). Simulation of ship propeller load based on MRASO-MPTC control, *Studies in Informatics and Control*, Vol. 33, No. 4, 73-82, doi:10.24846/v33i4y202407
[12] Özel, M. A.; Kopmaz, O. (2024). Design of a periodic structure for composite helicopter rotor blade, *International Journal of Simulation Modelling*, Vol. 23, No. 3, 447-458, doi:10.2507/IJSIMM23-3-692
[13] Wu, Z.; Bao, H.; Liu, L.; Xing, Y.; Huang, P.; Zhao, G. (2020). Numerical investigation of the performance of micro-textured cutting tools in cutting of Ti-6Al-4V alloys, *The International Journal of Advanced Manufacturing Technology*, Vol. 108, Nos. 1-2, 463-474, doi:10.1007/s00170-020-05428-1
[14] Xu, T.; Xie, L.; Ma, C.; Li, Q. (2025). Investigation of cutting performance of coated micro-textured tools for cutting aluminum alloys, *Mechanical Sciences*, Vol. 16, No. 1, 195-208, doi:10.5194/ms-16-195-2025
[15] Ma, J.; Duong, N. H.; Lei, S. (2015). 3D numerical investigation of the performance of microgroove textured cutting tool in dry machining of Ti-6Al-4V, *The International Journal of Advanced Manufacturing Technology*, Vol. 79, Nos. 5-8, 1313-1323, doi:10.1007/s00170-015-6937-1
[16] Zhang, G.-F.; Chen, B.-X.; Wu, G.; Xie, G.; Xie, H. (2022). Experimental assessment of textured tools with nano-lubricants in orthogonal cutting of titanium alloy, *Journal of Mechanical Science and Technology*, Vol. 36, No. 5, 2489-2497, doi:10.1007/s12206-022-0431-0
[17] Fouathiya, A.; Meziani, S.; Sahli, M.; Barrière, T. (2021). Experimental investigation of microtextured cutting tool performance in titanium alloy via turning, *Journal of Manufacturing Processes*, Vol. 69, 33-46, doi:10.1016/J.JMAPRO.2021.07.030
[18] Li, W.; Zhang, Z. (2019). Effect of cutting tool with micro-pits texture on wood cutting performance, *PLoS ONE*, Vol. 14, No. 4, Paper e0214888, 15 pages, doi:10.1371/journal.pone.0214888
[19] Cui, X. Y.; Li, Z. Z.; Yin, B. L.; Wang, W. Q.; Liu, Y. X.; Bai, Z. H. (2023). Modelling analysis of coupling deformation between strip steel and roller system, *International Journal of Simulation Modelling*, Vol. 22, No. 2, Paper 267-278, doi:10.2507/IJSIMM22-2-644

[20] Amin, M.; Rathore, M. F.; Ahmed, A. A.; Saleem, W.; Li, Q.; Israr, A. (2023). A feed direction cutting force prediction model and analysis for ceramic matrix composites C/SiC based on rotary ultrasonic profile milling, *Advances in Production Engineering & Management*, Vol. 18, No. 3, 288-302, doi:10.14743/apem2023.3.473
[21] Tong, X.; Han, P.; Yang, S.-C. (2022). Coating and micro-texture techniques for cutting tools, *Journal of Materials Science*, Vol. 57, No. 36, 17052-17104, doi:10.1007/s10853-022-07704-9
[22] Liu, W.; Tian, Z.; Xu, Y.; Zhao, M.; Li, R.; Pang, H.; Zhao, H.; Feng, Z. (2023). Drill string mechanics and extension capacity of extended-reach well, *Technical Gazette*, Vol. 30, No. 1, 39-51, doi:10.17559/TV-20220315014125
[23] Li, L.; Yang, D. L.; Cui, Y. M. (2023). Optimization of machining performance in deep hole boring: a study on cutting tool vibration and dynamic vibration absorber design, *Advances in Production Engineering & Management*, Vol. 18, No. 3, 371-380, doi:10.14743/apem2023.3.479
[24] Hao, X.; Cui, W; Li, L.; Li, H.; Khan, A. M.; He, N. (2018). Cutting performance of textured polycrystalline diamond tools with composite lyophilic/lyophobic wettabilities, *Journal of Materials Processing Technology*, Vol. 260, 1-8, doi:10.1016/j.jmatprotec.2018.04.049
[25] Zębala, W.; Kowalczyk, R. (2015). Estimating the effect of cutting data on surface roughness and cutting force during WC-Co turning with PCD tool using Taguchi design and ANOVA analysis, *The International Journal of Advanced Manufacturing Technology*, Vol. 77, Nos. 9-12, 2241-2256, doi:10.1007/s00170-014-6382-6
[26] Meng, X.; Lin, Y.; Mi, S. (2021). The research of tool wear mechanism for high-speed milling ADC12 aluminum alloy considering the cutting force effect, *Materials*, Vol. 14, No. 5, Paper 1054, 18 pages, doi:10.3390/ma14051054
[27] Pu, R.; Yu, Z.; Hao, X.; Yan, J.; Han, Z.; Tan, J.; Lu, L.; Chen, Z.; Yu, H. (2023). Effect of Si content on microstructure, mechanical properties, and cutting performance of TiSiN/AlTiN dual-layer coating, *Journal of Manufacturing Processes*, Vol. 88, 134-144, doi:10.1016/j.jmapro.2023.01.022